LS-DYNA® Smoothed Particle Galerkin (SPG) Method

Yong Guo[1], C.T. Wu[2] and Wei Hu[3]

[1]Senior Scientist and Presenting Author, Livermore Software Technology Corporation, 7374 Las Positas Road, Livermore, CA, 94551 USA. Email: yguo@lstc.com
[2]Senior Scientist, Livermore Software Technology Corporation, 7374 Las Positas Road, Livermore, CA, 94551 USA. Email: ctwu@lstc.com
[3]Scientist, Livermore Software Technology Corporation, 7374 Las Positas Road, Livermore, CA, 94551 USA. Email: whu@lstc.com

Abstract: A new particle method for large inelastic deformation and material failure analyses from low to moderated high speed applications is presented. The new formulation is established following a meshfree Galerkin approach for a solving of partial differential equation in solid mechanics problem. A nonlocal strain field is introduced to the formulation via displacement smoothing which is shown to be related to the least-square stabilization method for the elimination of zero-energy modes, the enhancement of coercivity and the introduction of non-locality in the particle methods [1]. The discretized system of equation is consistently derived within the meshfree Galerkin variational framework [2] and integrated using a direct nodal integration scheme. As fully Lagrangian kernel is incapable of simulating the severe deformation and material separation problem, the updated-Lagrangain kernel and Eulerian kernel [3-5] are developed to reset the reference configuration, maintain the injective deformation mapping at the particles and naturally handle the material separation due to damage. Both SMP and MPP simulations are available in the released LS-DYNA® version. Several numerical benchmarks and industrial applications are provided in this presentation to demonstrate the effectiveness and accuracy of the new method.

Kerwords: Meshfree method, nodal integration, stabilization, nonlinear

1 Introduction

Thanks for the characteristics of discretization flexibility and customized approximation, meshfree or particle methods have undergone extensive developments and led to widespread applications in interdisciplinary sciences and engineering over the past two decades. In particular, significant research efforts have been spent on the particle integration due to the conceptual simplicity and the reduced numerical restriction in modeling large deformation, moving discontinuity, and immersed problems in solid and structural applications.

Nevertheless, three types of instabilities [5] arise when a solid mechanics problem is solved by the particle method. Spurious energy mode in deformation is the first type of instabilities which mainly emanates from the rank instability [6] of the particle discrete

system. The rank instability is caused by the under-integration of weak forms inherent in the central difference formula from the direct particle integration scheme, and it requires numerical stabilization. Strain localization is driven by the material instability which presents the second type of instability in particle integration method. Physically, it is recognized [7] that the onset of strain localization in the rate-independent material coincides with the loss of ellipticity of the incremental problem. Mathematically, the strain localization leads to the ill-posedness of the incremental boundary value problem and requires a localization limiter [8]. Tension instability [9] is the third particle instability from discretization which results from the interaction of the second derivative of Eulerian kernel and the tensile stress [4]. Nowadays, the tensile instability can be entirely cured by an employment of Lagrangian kernels **Error! Reference source not found.** in the solid mechanics applications.

So far, several stabilization techniques have been developed to remove the spurious energy modes in the meshfree nodal integration solution. The meshfree Galerkin/least-squares (GLS) stabilization approach [6] presents a reconstructed weak form where a bilinear term consisting of the residual of equilibrium equation is employed to stabilize the solution. The principle drawback of this residual stabilization approach is the contradictory demands on the stabilization control parameter placed by accuracy requirement. Wu *et al.* **Error! Reference source not found.** developed the Smoothed Particle Galerkin (SPG) method in which a smoothed displacement field is introduced to stabilize the meshfree Galerkin nodal integration solution in large deformation and damage analyses. It was shown **Error! Reference source not found.** that SPG method is closely related to the nonlocal meshfree method [8] by means of strain regularization analysis. Their analysis results reveal the SPG method is developed based on a fully nonlocal model in strain approximation and can be used for the large strain analysis. In this paper, the LS-DYNA® SPG method is introduced to the severe deformation and material failure simulation, several related LS-DYNA keywords and their descriptions are also provided.

Our paper is organized as follows. In the next section, an overview on SPG method is given. The corresponding LS-DYNA® SPG keywords are given in Section 3. Numerical examples are presented in Section 4 to illustrate the robustness and accuracy of the proposed method. Section 5 concludes with a brief summary.

2 Overview on SPG Method

The explicit dynamic equation of the SPG method is described by [1-3]

$$\boldsymbol{A}^{-T}\boldsymbol{M}\boldsymbol{A}^{-1}\ddot{\bar{\boldsymbol{U}}} = \boldsymbol{A}^{-T}\left(\boldsymbol{f}^{ext} - \boldsymbol{f}^{\mathrm{int}}\right) \tag{1}$$

or equivalently

$$\boldsymbol{A}^{-T}\boldsymbol{M}\ddot{\tilde{\boldsymbol{U}}} = \boldsymbol{A}^{-T}\left(\boldsymbol{f}^{ext} - \boldsymbol{f}^{\mathrm{int}}\right) \tag{2}$$

where $\ddot{\bar{\boldsymbol{U}}}$ and $\ddot{\tilde{\boldsymbol{U}}}$ contains the vector of particle accelerations evaluated in the smoothed nodal position system and generalized nodal position system, respectively. $\boldsymbol{f}^{ext}$ and $\boldsymbol{f}^{Int}$

are corresponding external and internal force vectors, respectively. $\boldsymbol{M}$ is the consistent mass matrix given by

$$\boldsymbol{M}_{IJ} = \sum_{N=1}^{NP} \rho_0 \Psi_I(\boldsymbol{X}_N)\Psi_J(\boldsymbol{X}_N)V_N^0\boldsymbol{I} \tag{3}$$

where ρ_0 is the initial density, NP is the total number of particles, and $\Psi_I(\boldsymbol{X})$, $I=1,...NP$ can be considered as the shape functions of the meshfree approximation for displacement field. V_K^0 denotes the initial volume of particle K. $\boldsymbol{A}$ is a transformation matrix defined by

$$\boldsymbol{A}_{IJ} = \phi_J(\boldsymbol{X}_I)\boldsymbol{I} = \sum_{K=1}^{NP} \Psi_K(\boldsymbol{X}_I)\Psi_J(\boldsymbol{X}_K)\boldsymbol{I} \tag{4}$$

Eq. (1) also can rewritten as

$$\overline{\boldsymbol{M}}\ddot{\boldsymbol{U}} = \boldsymbol{A}^{-T}\left(\boldsymbol{f}^{ext} - \boldsymbol{f}^{\text{int}}\right) \tag{5}$$

with $\overline{\boldsymbol{M}} = \boldsymbol{A}^{-T}\boldsymbol{M}\boldsymbol{A}^{-1}$ defines a smoothed consist mass matrix. In explicit dynamic analysis a row-sum mass matrix is usually considered which is only computed once without involving matrix inversion at each time step. The smoothed consist mass matrix is now replaced by the row-sum mass matrix $\overline{\boldsymbol{M}}^{RS}$ to give

$$\overline{\boldsymbol{M}}_I^{RS} = \sum_J^{NP} \overline{\boldsymbol{M}}_{IJ} = \sum_J^{NP} \boldsymbol{A}_{IK}^{-T}\boldsymbol{M}_{KM}\boldsymbol{A}_{ML}^{-1} \tag{5}$$

As Lagrangian simulation proceeds, an updated Lagrangian/Eulerian kernel scheme is performed frequently to avoid the negative Jacobian in the Lagrangian calculation. In each adaptive step material quantities are computed at particles without the usage of background cells. Since the updated Lagrangian/Eulerian kernel approach does not involve remeshing and particle computation is evaluated node-wise, the material quantities at all particles are maintained in the Lagrangian setting and thus require no remap procedures. If we denote the variables before and after the each adaptive time step to be superscripted with "–"and "+" respectively, the derivatives of material meshfree shape functions with respect to spatial coordinates right before $(k+1)$-th adaptive time step can be expressed by

$$\Psi_{I,i}^{-}\left(\boldsymbol{x}^{k+1}\right) = \frac{\partial \Psi_I^{-}\left(\boldsymbol{x}^{k+1}\right)}{\partial x_i^{k+1}} = \frac{\partial \Psi_I^{-}\left(\boldsymbol{x}^{k+1}\right)}{\partial x_j^{k}}\frac{\partial x_j^k}{\partial x_j^{k+1}} = \frac{\partial \Psi_I^{-}}{\partial x_j^k} f_{ji}^{k^{-1}} \tag{6}$$

where $f_{ji}^{k^{-1}} = \dfrac{\partial x_j^k}{\partial x_j^{k+1}}$ defines the inverse of incremental deformation gradient from k-th adaptive time step. At $(k+1)$-th adaptive time step, the new derivatives of material meshfree shape functions becomes

$$\Psi_{I,i}^{+}\left(\boldsymbol{x}^{k+1}\right)=\frac{\partial\Psi_{I}^{+}\left(\boldsymbol{x}^{k+1}\right)}{\partial x_{i}} \tag{7}$$

Since no remap procedures are considered in the adaptive step, the particle mass is taken to be the same during the explicit dynamics analysis. The current particle volume required for the calculation of internal force is updated according to the continuity equation given by

$$V_{I}=\frac{\rho_{0}}{\rho_{I}}V_{I}^{0} \tag{8}$$

$$\frac{d\rho_{I}}{dt}=-\rho_{I}\nabla\cdot\left(\tilde{\dot{\boldsymbol{u}}}_{I}\right)=-\rho_{I}\sum_{J=1}^{NP}\tilde{\dot{\boldsymbol{u}}}_{J}\cdot\Psi_{J,\boldsymbol{x}}\left(\boldsymbol{x}_{I}\right) \tag{9}$$

In LS-DYNA®, we consider the adaptive step be periodically taken by a constant time interval. Figure 1 illustrates the evolution of updated Lagrangian/Eulerian kernel in one adaptive step.

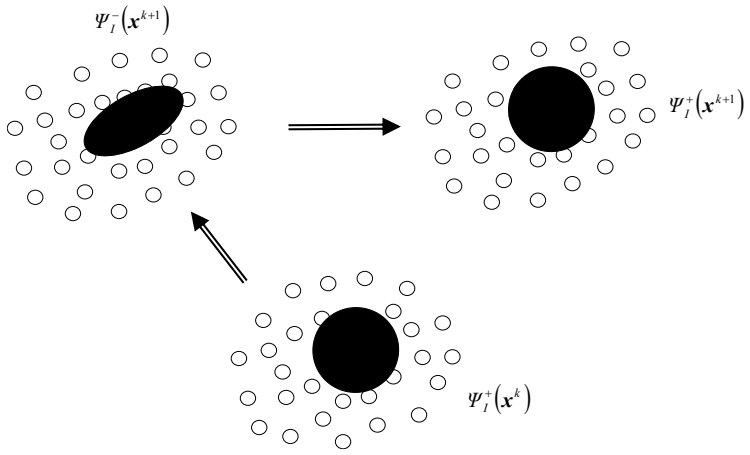

Figure 1. The evolution of updated Lagrangian/Eulerian kernel in the adaptive scheme.

3 LS-DYNA® SPG Keywords

4 Numerical Examples

4.1 Material failure simulation in a 3D plate

To demonstrate the applicability of SPG in the general three-dimensional problem, the material failure of a metal plate is simulated. The 3D metal plate has a size of 0.2m in diameter and 0.023m in thickness. It is subjected to an indentation of ball with a size of 0.03m in diameter. The ball is assumed to be rigid and is traveling at a constant speed of 0.893m/s. The material constants of the metal bar are [12]: Young's modulus E=206.9 GPa, Poisson's ratio ν=0.29, density ρ^{0}=7860 kg/m^3 and the isotropic hardening rule

$\sigma_y(\bar{e}^p)=\sigma_y^0+\alpha\bar{e}^p+(\sigma_y^\infty-\sigma_y^0)(1-e^{-\beta\bar{e}^p})$ with coefficients β=16.93, σ_y^0 =0.45 GPa, σ_y^∞ = 0.715 GPa and α =0.12924 GPa. The 3D plate is discretized by the finite element analysis model which is composed of 35470 hexahedra elements (39941 nodes) as shown in Figure 2.

The progressive deformed geometries are plotted in Figures 3. Figure 4 presents the load-displacement response. xxxxxxxx

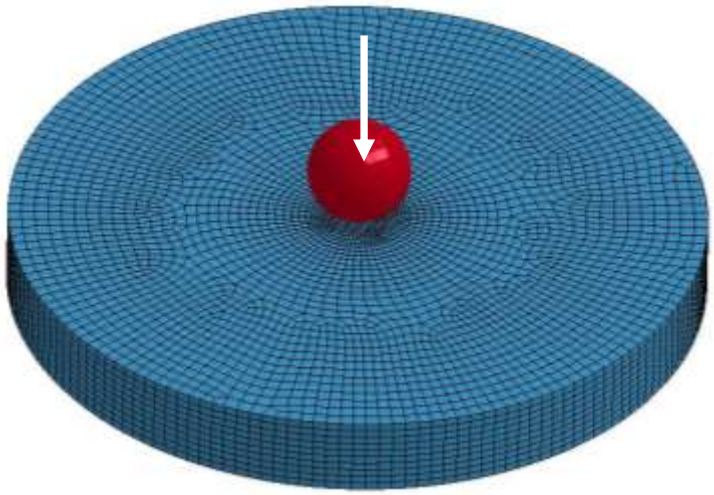

Figure 2. The finite element mesh of 3D metal plate in material failure problem.

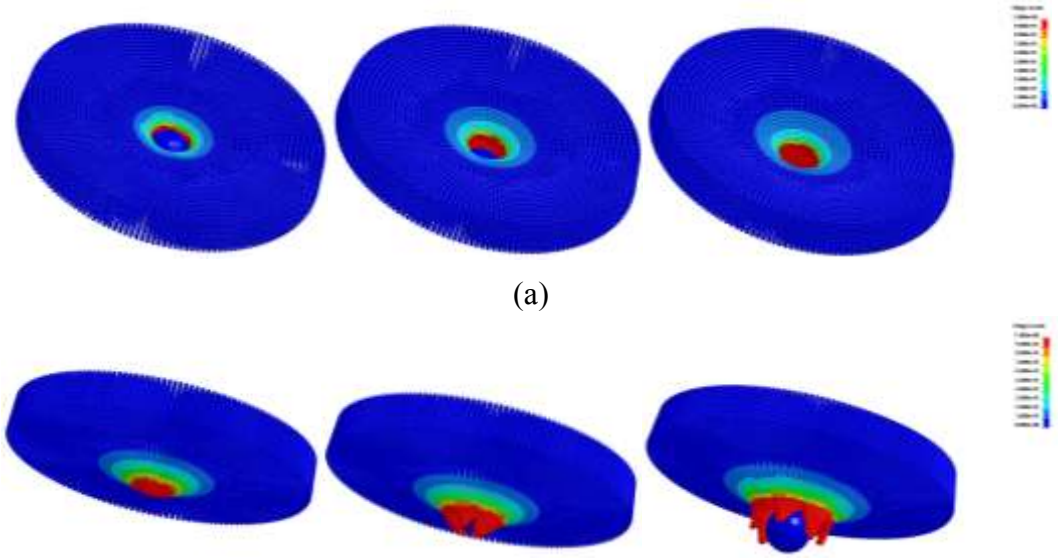

(a)

(b)

Figure 3. Deformed configuration of 3D plate in effective plastic strain contour: (a) top view; (b) bottom view.

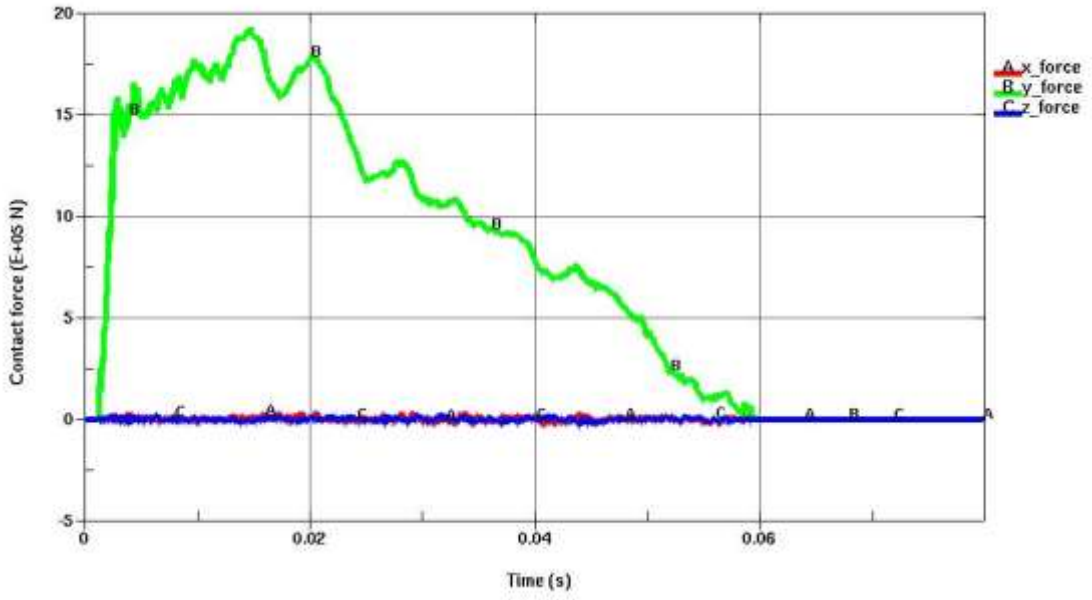

Figure 4. Force response of the contact force in failure simulation.

4.2. 3D metal grooving simulation

This problem is studied to identify the applicability of SPG method in three-dimensional severe deformation analysis. A metal block of size 0.1 m × 0.06 m × 0.02 m is fixed at the bottom and grooved by a rigid rotating roller as shown in Figure 5. The width of the roller is 0.008 m. The roller has a constant rotating speed w=125 rad/s and is traveling at a transverse speed V=0.5 m/s. For present purpose, we further assume the grooving process is isothermal and frictional coefficient for the contact between roller and work piece is 0.1. The material has an initial density ρ^0 = 2700 kg/m^3. The strain-hardening elastic-plastic material properties are: Young's modulus E=70.0 GPa, Poisson's ratio v=0.3, and an isotropic hardening rule $\sigma_y\left(\bar{e}^p\right)=\sigma_y^0+\gamma E_p\bar{e}^p$ with coefficients γ=1.0, σ_y^0=0.1 GPa, and E_p=1.5e-2 GPa. The finite element analysis model for the work piece contains 15000 hexahedra elements (17391 nodes) which are uniformly distributed as shown in Figure 5. For finite element methods, both one-point integration with hourglass control formulation (FEM1) and selective reduced integration formulation (FEM2) are considered for the comparison. Explicit dynamics analysis is conducted for this simulation.

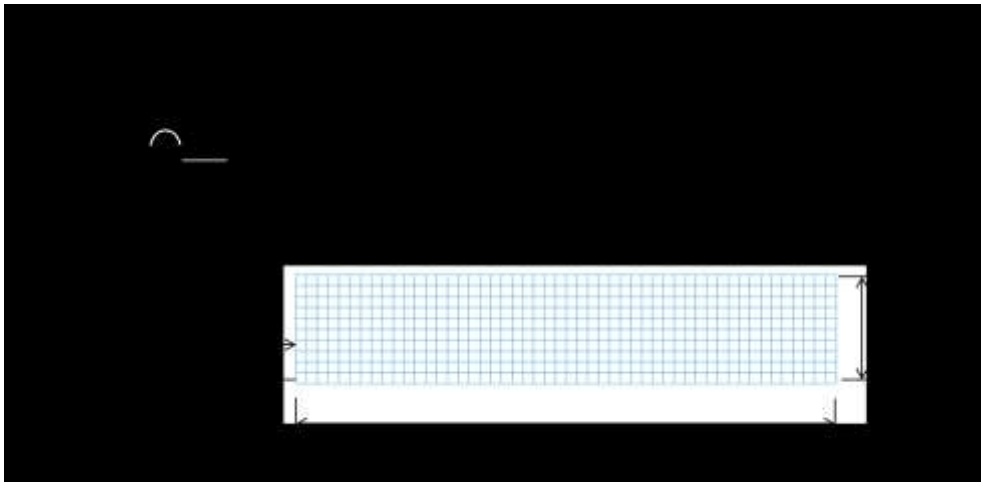

Figure 5. 3D metal grooving problem.

The final deformed geometries with effective plastic strain contours are plotted in Figures 6 (a)-(c) for the FEM2, FEM1 and SPG method, respectively. As shown in Figure 6 (a), FEM2 method experiences severe mesh distortion problem and the simulation stops in the early stage. Surprisingly, the FEM1 method improves the simulation in FEM2 and completes two-thirds of the simulation in grooving process as shown in Figure 6 (b). On the other hand, the SPG method is able to accomplish the grooving simulation as depicted in Figure 6 (c) for the final deformed geometry. It is worthwhile to note that the SPG method is very stable and no shooting nodes are observed in the simulation. The comparisons of contact force in vertical and longitudinal directions are given in Figures 7 (a) and (b), respectively. Good agreement between FEM1 solution and the SPG solution is shown in the plunging phase and steady state of the grooving phase before roller retracts. In contrast, the negative volume causes the FEM2 simulation to abort early in the plunging phase as shown in the contact force response.

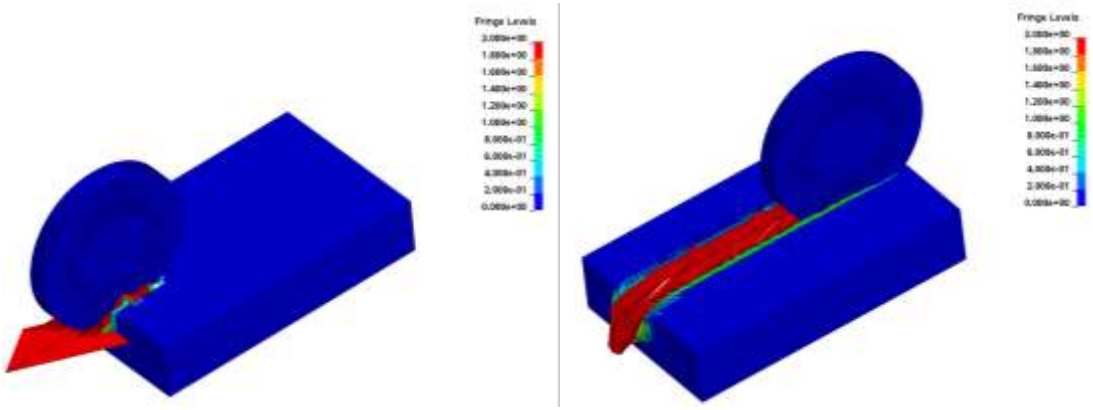

(a) (b)

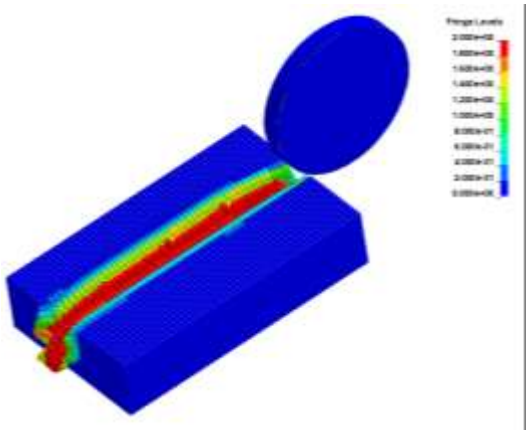

(c)

Figure 6. Final deformation in the grooving problem: (a) FEM2; (b) FEM1; and (c) present method.

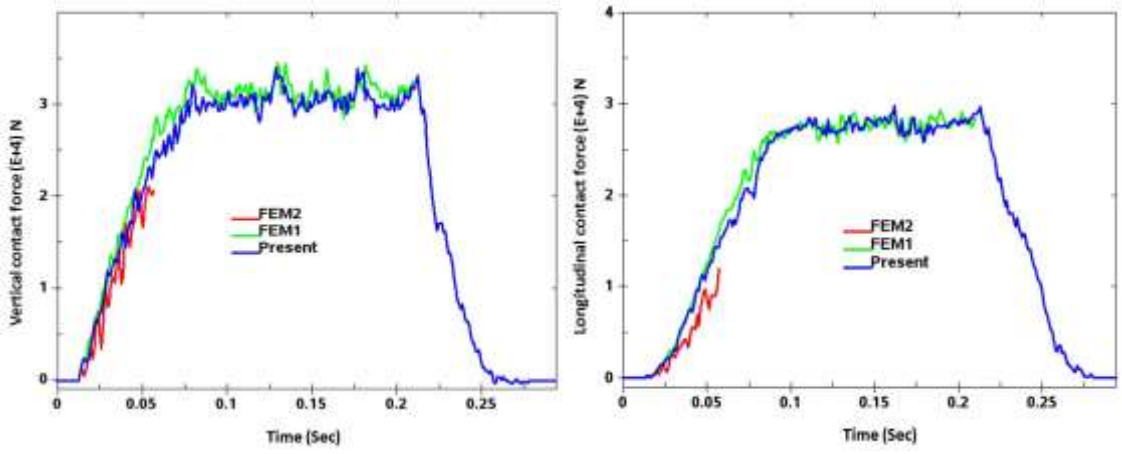

(a) (b)

Figure 7. Comparison of contact force in the grooving problem: (a) vertical direction; and (b) longitudinal direction.

To study the effect of material failure in grooving simulation, the Eulerian kernel is adopted (IDAM=1) and failure criteria (fs=0.3) is considered. The final deformed geometry with effective plastic strain contours are plotted in Figures 8 (a) and (b) for the SPG method without and with material failure, respectively. The maximum range of the effective plastic strain contour plot in Figure 8 is 0.3. Apparently, the influence region of effective plastic strain in the case of damage model is more profound than that of non-damage model. The difference can be verified on their contact force responses as shown in Figures 9 (a) and (b) for the vertical and longitudinal directions, respectively. As it is shown in Figure 9, the contact forces in both vertical and longitudinal directions reduce in the damage case particularly during the steady state of the grooving process. The reduction of contact force response in the longitudinal direction is more evident than the vertical direction. This is due to the potential loss of frictional contact caused by the material failure on the grooving surface.

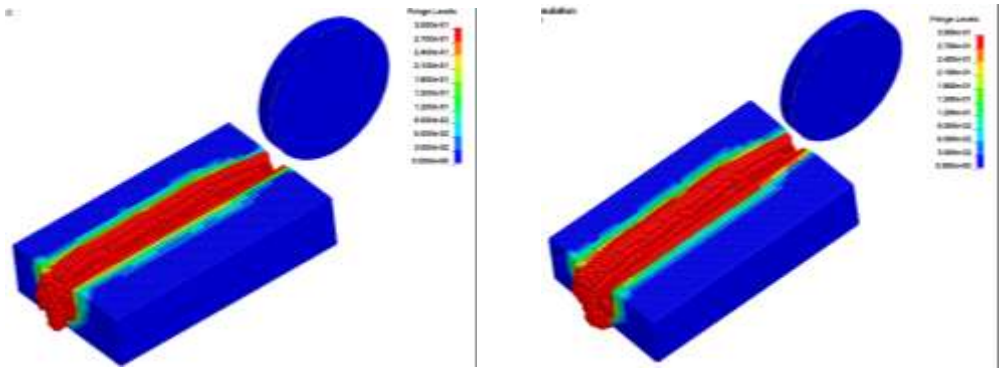

(a) (b)

Figure 8. Final deformation in the SPG grooving simulation: (a) non-damage; and (b) damage.

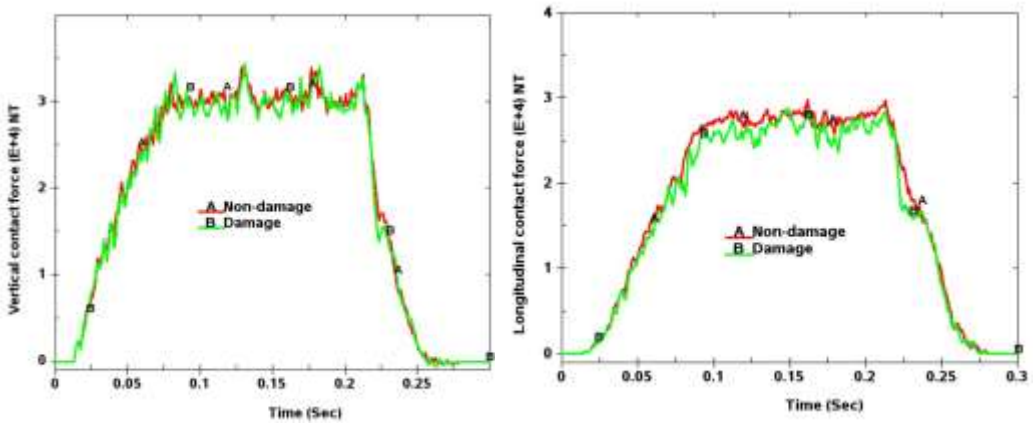

(b) (b)

Figure 9. Comparison of contact force in the SPG grooving simulation: (a) vertical direction; and (b) longitudinal direction.

5 Conclusion

A stable and accurate particle method is attractive from the viewpoint of formulation simplicity and simulation capability in the nonlinear analysis of solid mechanics problems. In this paper, the LS-DYNA® SPG method is introduced which is free from stabilization control parameters and integration cells for the particle computation. Several kernel formulations have been incorporated into the nonlinear SPG formulation to enhance the simulation capability for severe deformation and damage analysis.

[1] Wu C.T., Guo Y., Hu W. An introduction to the LS-DYNA smoothed particle Galerkin method for severe deformation and failure analysis in solids. 13th International LS-DYNA Users Conference, Detroit, MI, June 8-10, 1-20, 2014.
[2] Wu C.T., Hu W., Koishi M. (2015) A smoothed particle Galerkin formulation for

extreme material flow analysis in bulk forming applications. *International Journal of Computational Methods*, Accepted for publication.

[3] Wu C.T., Koishi M., Hu W. (2015) A displacement smoothing induced strain gradient stabilization for the meshfree Galerkin nodal integration method. *Computational Mechanics,* Vol. 56 (1), pp. 19-37.

[4] Wu C.T., Wang D.D., Guo Y. (2015) An immersed particle modeling technique for the three-dimensional large strain simulation of particulate-reinforced metal-matrix composites, *Applied Mathematical Modelling*, Accepted for publication.

[5] Belytschko T., Guo Y, Liu, W.K, Xiao S.P. (2000) A unified stability analysis of meshless particle methods. *International for Numerical Methods in Engineering,* Vol. 48, pp. 1359-1400.

[6] Beissel S., Belytschko T. (1996) Nodal integration of the element-free Galerkin method. Computer Methods in Applied Mechanics and Engineering Vol. 139, pp. 49-74.

[7] Hill R. (1962) Acceleration waves in solids. *Journal of Mechics and Physics of Solids*, Vol. 10, pp. 1-16.

[8] Chen J.S., Wu C.T., Belytschko T. (2000) Regularization of material instabilities by meshfree approximations with intrinsic length scales. *International for Numerical Methods in Engineering,* Vol. 47, pp. 1303-1322.

[9] Dyka, C.T., Randles P.W., Ingel R.P., (1997) Stress points for tension instability in SPH, *International for Numerical Methods in Engineering* Vol. 40, pp.2325-2341.

[10] Belytschko T., Guo Y., Liu W.K., Xiao S.P. (2000) A unified stability analysis of meshless particle methods. *International for Numerical Methods in Engineering* Vol. 48, pp. 1359-1400.